

A Double-layered Timber Plate Shell - Computational Methods for Assembly, Prefabrication and Structural Design

Christopher Robeller, Mina Konakovic, Mira Dedijer, Mark Pauly and Yves Weinand

Abstract. *This paper presents a new lightweight construction system for doubly-curved shells, built from two interconnected layers of structural wood veneer plates. The system uses integral through-tenon joints for a fast, precise, and simple assembly, allowing for the construction of a series of differently shaped shells without a costly mould or support structure. Instead, inclined joints cut with a 5-axis CNC milling machine embed the correct location and angle between plates into the shape of the parts. This constrains the relative motions between joined parts to one assembly path.*

To take advantage of the benefits of such connectors, the constrained assembly paths must be considered in the fundamental design of the system, allowing for the insertion of each plate. This imposes additional constraints in the segmentation process of doubly-curved shells. In order to meet the requirements and resolve the multi-constraint system, we use a global, nonlinear optimization approach.

Developed as a close collaboration between architects, computer scientists and structural engineers, the paper includes an experimental analysis of the influence of parametric modifications in the shape of connectors on their load-bearing performance.

1 Introduction

The use of CNC-fabricated integral joints, such as through-tenons and dovetails, is a common technique in modern timber frame constructions with linear members such as beams and posts. These connectors allow for a fast, precise and simple on-site assembly, taking advantage of prefabrication technology, reducing and replacing increasingly expensive manual labour.

An innovative application of such joints is the construction of freeform timber plate structures, which have been the subject of recent research in the field of architectural geometry. Examples are the single-layered and double-layered Timber Folded Plate Structures [Robeller and Weinand 2015] [Robeller and Weinand 2016b] or the ICD/itke Landegsgartenschau Pavilion [Krieg et al. 2015] [Li and Knippers 2015]. In such designs, structurally beneficial curved or folded shapes are constructed from hundreds or thousands of small and individually shaped, planar plates, made from cross-laminated wood panels such as laminated veneer lumber (LVL).

The design and fabrication of such structures is made possible by CAD programming interfaces and automatic fabrication technology. However, the assembly of the parts on site is still carried out manually. Locator features, which constrain the relative movements of parts to only one possible assembly direction (1DOF) are crucial for a fast and precise assembly of such complex designs. They allow reducing or completely replacing the need of costly support structures or moulds that prescribe the shape of the freeform structure.

In addition to the improved assembly, the previous research projects have also demonstrated that integral joints can be used to transfer forces between the plates, reducing or replacing additional connectors such as screws or nails.

This paper builds upon the previous research, demonstrating a new construction system for a double-curved shell structure built from two interconnected layers of thin LVL panels, assembled entirely with 1DOF closed-slot joints. The construction system with two thin layers takes particular advantage of the new possibility for the edgewise connection of thin plates with integral joints.

2 Project Description

The construction for a timber prefabrication facility covers an area of $5.800m^2$ with a series of 23 discontinuous shells, each 6m wide and 9m high (Figure 1). In the transversal direction of the shells, an s-shaped cross-section curve introduces a second curvature which prevents buckling, the expected mode of failure for such a structure. [Pedreschi and Theodossopoulos 2007]

The design was inspired by the famous *Gaussian Vault* masonry roof structures of the Uruguayan architect and engineer Eladio Dieste, such as the TEM factory in Montevideo, Uruguay, 1960-1962, and the Caese Produce Market in Porto Alegre, Brazil, 1969-1972. [Anderson 2004]

In addition to the structural advantages of the doubly-curved shape, it is also essential for the architectural concept. Multiple, successive shells with such a cross-section create an overlap in between, which is used as a clerestory for the natural lighting and shading of the building, much like the sawtooth roofs of 19th century factories.

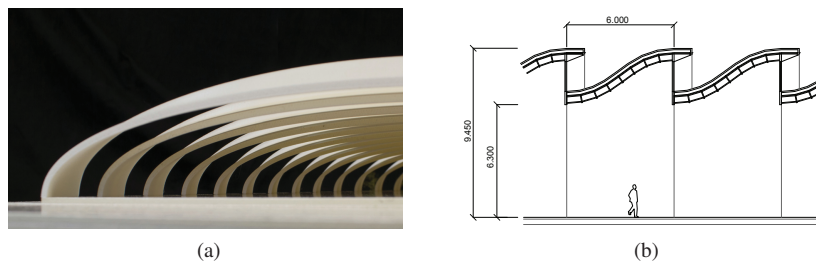


Figure 1: Interior View and Cross-section schematic

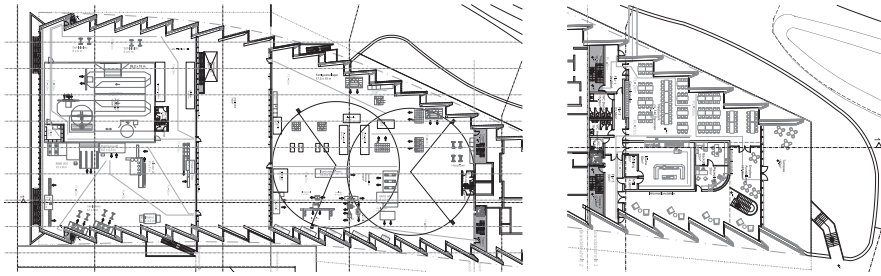


Figure 2: Floor plans left: production spaces, right ground floor offices

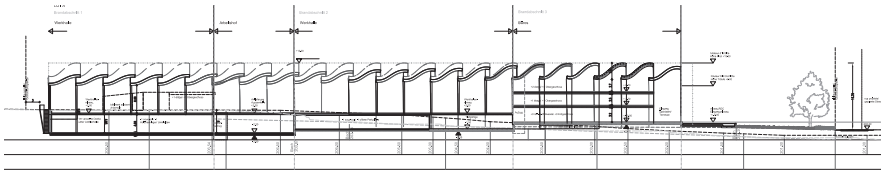


Figure 3: Cross section through the building

However, in contrast to the Dieste's structures, where a series of shells with the same shape was built through the repetitive use of a single mould or template, our project requires the construction of 23 individually shaped shells. This is both due to the shape of the building site, which is not rectangular but obtuse trapezoidal, and the architectural program, merging from a single-story factory space on the southern wide end into a triple-storey office area at the narrow northern end of the site (Figures 2 and 3).

The span of the shells ranges from 22.5m in the smallest, to 53.7m in the largest shell. The cross-section profile in this main direction of loading is a compromise between the architectural program and a structurally optimized shape. With a span-to-rise ratio of 2.5 - 6, it deviates from the catenary line, which Dieste used for his masonry roofs (with a span-to-rise of 8-10), mostly in the first 4 meters from the ground plane. Here our shells are tangential to the vertical axis, reducing horizontal forces on the supports.

3 Construction System

Our system consists of two layers of thin plates, instead of one thick layer, taking advantage of our joints' ability to connect thin plates, which already provide a high strength but are difficult to join with conventional fasteners such as screws.

A double-layered prototype was demonstrated in the ICD/itke Research Pavilion 2011 [la Magna et al. 2013], where prefabricated polyhedra made from wood veneer plates with finger joints (3DOF) were assembled to a spatial structure. In contrast

to this project, our system uses 1DOF integral joints not only within segments / modules (in the previously mentioned project, prefabricated modules were joined with metal connectors), but between all of the plates, in order to take advantage of the locator and connector features everywhere in the structure.

Figure 4a shows our construction system, which approximates the curved target surface with hexahedra-shaped segments S_i , each consisting of four plates. Each segment is based on a center point P_i and a normal vector \vec{n}_i . A combination of multiple parameters in the system allows for the rotation between the normal vectors of neighboring segments, which is required by the curvature of the target surface.

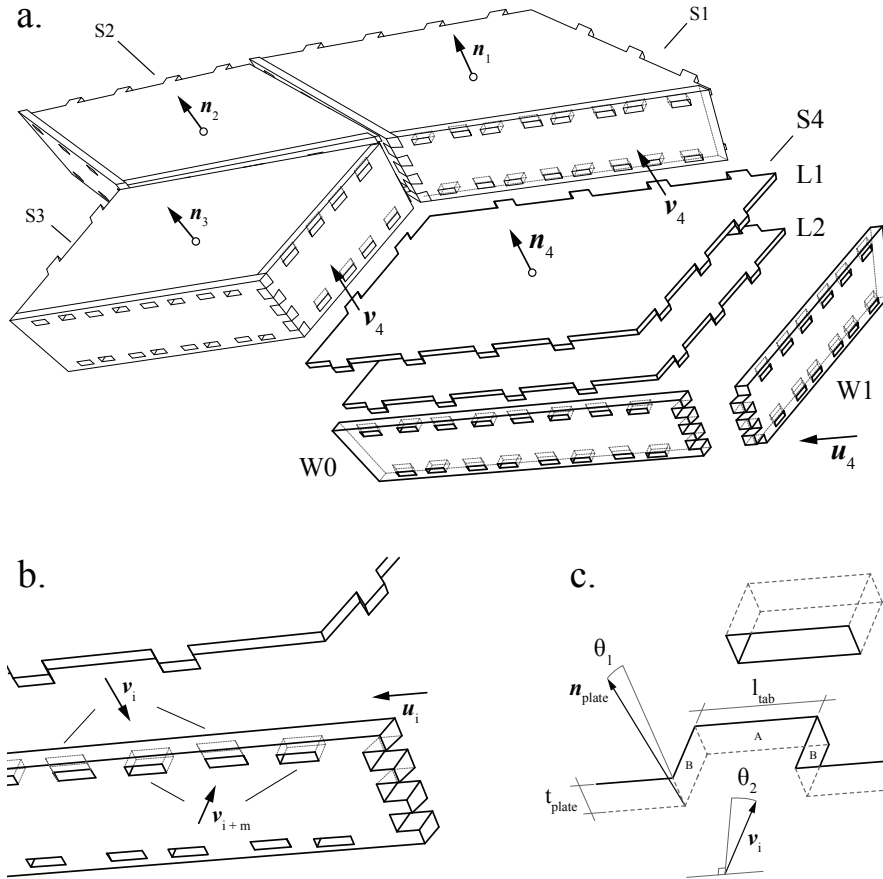


Figure 4: Construction system for a 2-layered shell, a: assembly of 4-sided box segments, b: alternating allocation of joint slots on shared vertical plates, c: joint detail / rotations

Within each segment, there are two shell plates, parallel to the segment plane, ($L1$ and $L2$) which form the two layers of the shell structure. Two additional vertical shear block plates $W0$ and $W1$ are used to transfer forces between the two layers of

the shell. There are no plates for the remaining two vertical faces of the hexahedron, because these plates are shared with the neighboring segments.

Figure 4b shows how a vertical plate supports the connection of the main layers of the shell: The intersection area of the three plates is divided into alternating segments, creating slots which receive the tabs of the shell plates. This allows for a direct contact between the shell plates for the transfer of compressive forces. In between these slots and on the top and bottom face of all tabs, the vertical plate holds the shell plates.

The assembly of the segments follows their numbering. Figure 4 shows the assembly of Segment S_4 in an $m \times n$ matrix of segments. Within a segment, the shell plates are inserted first, along the segment's assembly vector \vec{v}_i . They connect simultaneously to the two shear block plates of the neighboring segments S_{i-1} and S_{i-m} . The slots in these neighboring shear plates are oriented along \vec{v}_i , to receive the tenons of the shell plates $L1_i$ and $L2_i$.

3.1 Joints

Figure 4c shows a close-up view of the through-tenon joints that connect the shell plates. We have chosen these so called closed-slot connectors, because they combine the benefits of dovetail joints with additional features. Like the dovetails, the shape of the through-tenon joint are kinematically classified as prismatic pins with slots, constraining the Mobility of parts to one assembly motion path ($M = 1$) [Whitney 2004]. This shape fully integrates a unique position of the parts within the structure and allows for a rapid and precise assembly.

While the 1DOF property is also provided by open-slot dovetail joints, through-tenon joints provide additional features for the transfer of forces. The bending strength of different types of multiple-tab-and-slot plate joints (MTSJ) has been compared by [Roche et al. 2015a], demonstrating that joints with a closed slot, also called through-tenon joints, combine the high shear strength of finger- and dovetail joints (see [Roche et al. 2015b]) with a high bending strength.

Like dovetail joints, through-tenon joints connect plates in two planes. The average dihedral angle $\varphi_{mean} = 6.5^\circ$ between our shell plates is too small for the use of such joints. We solve this problem with the connection through the vertical shear plates in between shell plates. This connection requires only a small rotation θ_1 of the joint faces about the edge line (see Figure 4c, faces marked A).

However, the assembly of our system requires a second rotation of the tabs θ_2 , about the normal vector of the plate, because we want to connect two non-parallel edges simultaneously, along the same direction \vec{v}_i .

This rotation θ_2 has an influence on the shear strength of the joints, which we have analyzed. Figure 5 shows our shear load test, where we have examined a joint with two tabs at a rotation θ_2 from 10° to 40° , with the load applied in both directions. Graph 5b shows that the best shear strength is achieved at low rotations up to 25° , although the larger rotations of 25° to 40° also show a satisfying shear stiffness. Most specimen showed a brittle failure, while some specimen with angles larger than 30° showed a certain amount of hardening after the failure. The bottom

graph shows the load/displacement behaviour in the linear elastic range of 10-40%.

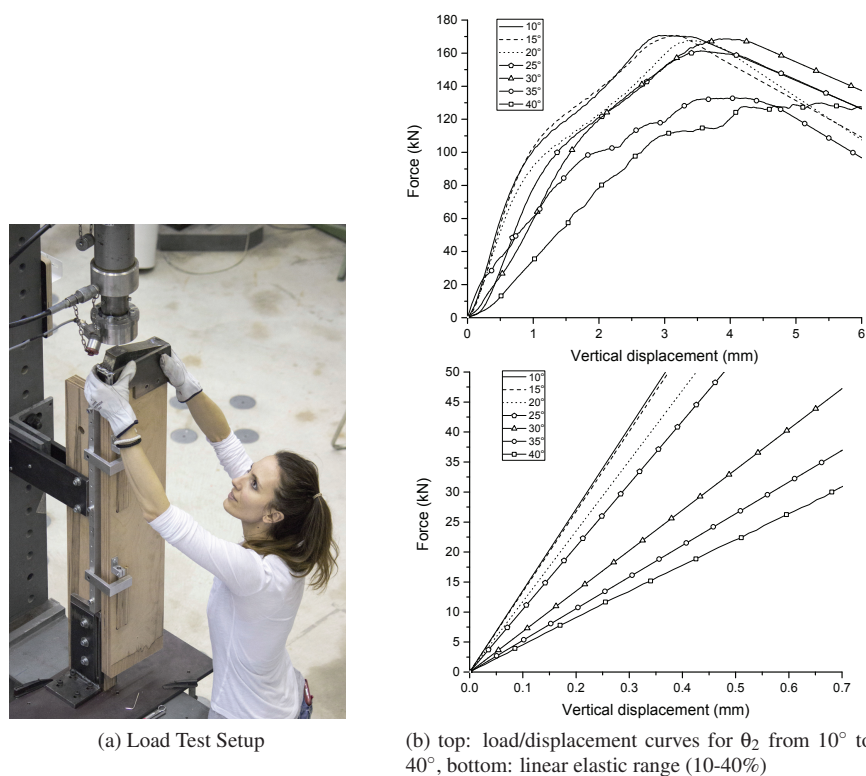


Figure 5: Experimental analysis of the influence of the tab rotation θ_2 on the shear stiffness of the joints on 40mm cross-laminated LVL plates.

Figure 6 illustrates the contact surfaces between two 40mm thick shell plates, along an edge with a length of 1.65m. Without integral joints, the contact area between these plates is 662cm^2 . In our system, neighboring edges are slightly rotated, Figure 6 shows an example where this angle is $\kappa = 0.82^\circ$. Without joints, this rotation reduces the contact area to 85.1%. With our integral joints (Figure 6b), the frontal contacts (for the transfer of compression) are divided into a direct and indirect area. Through the front face of the tabs, plates are in direct contact on 222cm^2 (33.5%). Additionally, an indirect contact of 383cm^2 (57.5%) is established through the vertical shear plate, adding up to 605cm^2 (91% of max area of two parallel edges). A distinction between the two areas is made because of the fiber direction of the wood plates. The indirect compression is transferred normal to the shear plate, where the compressibility strength is reduced. (Figure 6, left)

Additionally the joints provide a large contact area transversal to the edge. In Figure 6, there is an additional 220cm^2 (+33%) across the plate surface, which is relevant for shear forces, and 597cm^2 (+90%) parallel to the plate, which is rele-

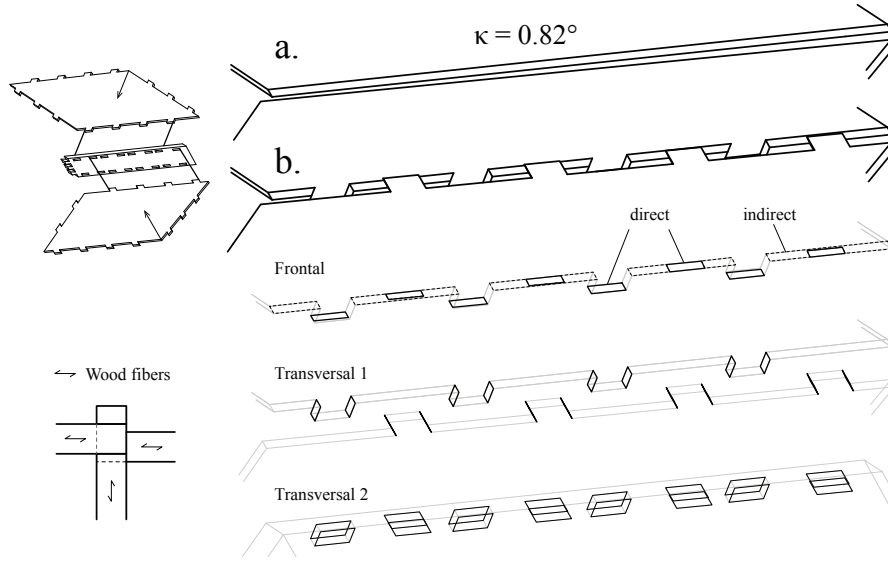


Figure 6: Contact area between two shell plates, without (a) and with joints (b)

vant for bending moments. The total contact area between the plates with joints is $1,422\text{cm}^2$ (214%).

3.2 Assembly-constrained Tiling

For our assembly of multiple parts, where the mobility of each part is reduced to $M = 1$, we must find a solution where each part can be inserted without conflicts.

Additional constraints are that we want to insert each part individually, and we want to use the interlocking of elements to block the last degree of freedom of the parts with one another, avoiding long-range escape paths in the assembly, which allow for multiple segments to be detached simultaneously.

The assembly path \vec{v}_i of parts is considered an *Escape Path* for the part. A part is considered *locally free*, when the escape path of all of its connections have a common direction. In this case, the dot product of all escape paths is 1, assuming \vec{v}_i as unit vectors. If this is not the case, the part is blocked and cannot be removed without prior removing other parts from the assembly. A second important situation is *global freedom*, also called long range escape paths, where a group consisting of multiple parts can be separated from the assembly along one common direction.

Figure 7 illustrates the assembly of 4×2 quadrilaterals with different shapes. Figure 7a uses rectangles with prismatic pins perpendicular to their edges. In this assembly all eight pieces are locally blocked, meaning that no single element such as part A can be removed. In order to remove A, we have to either remove the four parts E, F, G, H, or we remove A together with part E, which shows the existence of a long range escape path in this assembly. For our construction this pattern has two

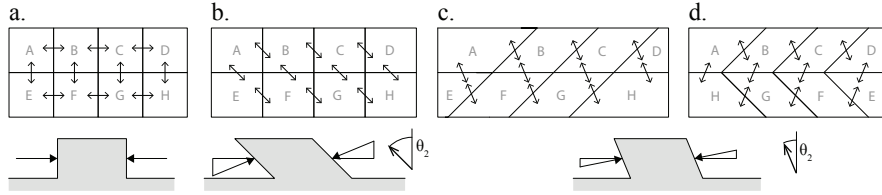


Figure 7: Comparison of different patterns from a point of view of assembly and transfer of forces: a. rectangular elements with pins perpendicular to the edges, b. rectangular elements with parallel pins, c. rhombus-shaped elements with parallel pins, d. rhombus-shaped elements with parallel pins, alternating orientation for every second row (Herringbone Pattern).

major disadvantages. The assembly of this configuration is only possible by first connecting all elements in the first row A, B, C, D , then connecting all elements in the second row E, F, G, H , and finally connecting the two groups. This means that in the final step, the edges of four elements must be joined simultaneously, which is problematic due to the combined length of this edge, which needs to be kept parallel during the assembly. Also, tolerances of the parts themselves and caused by the connections within the two groups will make it difficult to assemble these two groups in one step.

These problems can be resolved through pins which are not perpendicular to the edges, but rotated to share one common direction per segment (Figure 7b).

The required rotation of the pins θ_2 can be obtained from the angle α between the edges which are connected simultaneously as $\theta_2 = 90^\circ - (\alpha/2)$. For the array of rectangles shown in Figure 7b, all pins must be rotated at $\theta = 45^\circ$. As discussed in section 3.1, we want to avoid such large rotations on our joints.

We solve this problem through the use of *rhombus shaped* elements, as shown in Figure 7c. With $\alpha = 135^\circ$, we can reduce the rotation of the pins to 22.5° , half of the previous value using rectangles. However, while this configuration allows to assemble the array piece by piece, and the shape of the elements greatly reduces the required rotation of the pins, all three configurations shown in Figure 7a,b,c share a common problem of multiple long range escape paths.

This problem is greatly reduced by the *fishbone* pattern configuration in Figure 7d, where every second row of the rhombus shaped elements is mirrored. In consequence the assembly direction is also reversed in all mirrored rows.

Except for the last row, all elements in such a configuration are connected with multiple pins with different directions, similar to the configuration a., but with the possibility of piece-by-piece assembly and without any escape paths in the vertical direction.

3.3 Application to target surface

In order to create a two layer shell structure, we first need to segment a given design surface. To apply the previously chosen tiling pattern to our doubly curved target

surface, we use a first algorithm to generate the basic pattern through the evaluation of a point grid on a NURBS surface.

We gradually increase the density of this point grid in the main direction of loading, starting with a quadratic 500 x 500mm segment on the ground plane, with a linear increase to a maximum segment size of 500 x 2,500mm at the top of the shell. This relates both to the increased curvature on the lower end of the shells (see the curvature graphs in Figure 8), as well as the increased loads in this area. With this subdivision, we obtain a quad mesh for each shell, with 312 faces on the first shell, and 216 faces on the last one.

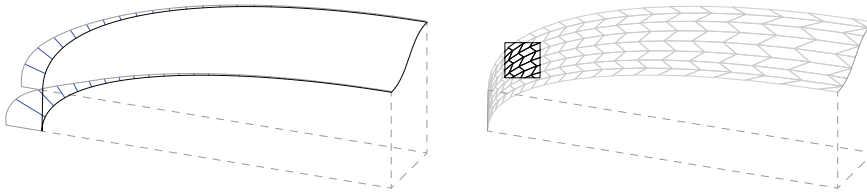


Figure 8: Left: Isometric view of the first shell. The length of the blue lines illustrates the curvature of the rail curves in main direction of loading. Right: Tiling of the first shell.

Each quad mesh of this basic pattern lies exactly on the target surface, but the quadrangular faces are not planar. Unlike in constructions with glass or metal panels, where a certain amount of non-planarity is permissible, we require very close to 100% planarity of the segments, due to the high rigidity of the 40mm thick structural wood veneer panels (LVL) that we use for our construction. These plates do not allow for any significant bending or twisting.

Planar quad meshing has recently been an active area of research, see [Pottmann et al. 2015] for an overview. A common approach relies on the fact that planar quad meshes can be interpreted as discrete versions of conjugate curve networks [Liu et al. 2006]. Such methods therefore optimize for the alignment of mesh edges with discrete approximations of conjugate curves. In our case study, however, the chosen tiling pattern in general does not follow conjugate directions. To overcome this problem, we do not represent our plate structure as a quadrilateral mesh, but as a collection of disconnected, but spatially coupled, planar elements. This introduces additional degrees of freedom for our global optimization that tries to approximate the target surface as well as possible, while respecting all the fabrication and assembly constraints.

Our solution is based on the geometric optimization framework proposed by [Bouaziz et al. 2012] and [Deuss et al. 2015]. The core of this method is an iterative solver that minimizes a global non-linear energy function derived from a suitable chosen set of geometric constraints. A key feature is that constraints can be implemented via local projections that provide a modular mechanism to satisfy each constraint locally. A global step then reconciles all these local projections in a least-squares sense. Global optimization distributes the error across the surface and thus

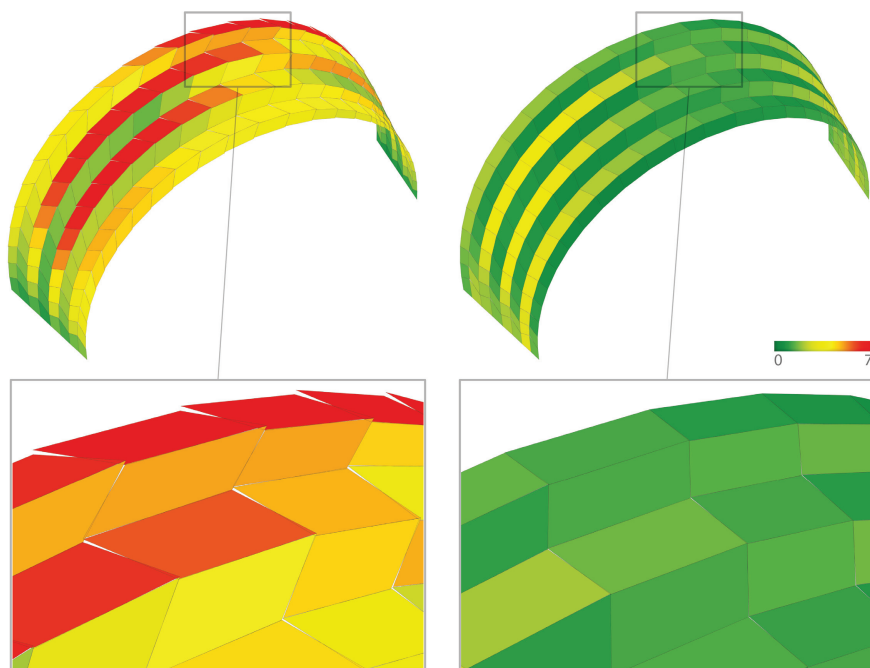


Figure 9: Comparison of a local and a global optimization approach applied on the last shell. Quad faces are colored according to a maximal angle κ between the edges of neighboring faces. The angle varies from 0 to 7 degrees. Left: By planarizing each face independently average κ angle is 2.05 degrees and maximal κ angle is 7. Right: Our global approach can reduce the average κ angle to 1.03 degrees, and the maximal angle to 3.72.



Figure 10: Balancing the fabrication requirements with the optimization. From left to right different optimization results are given by controlling the weights of constraints. First row is the top view and the second row is the side view of the last shell. Meshes are colored according to a maximal angle κ between the edges of neighboring faces. The comparison of κ angle, α angle, and deviation from the target surface is given in Table 1.

significantly decreases locally undesirable behavior, such as large angles κ between neighboring edges (see section 3.1). A comparison with a simple local optimization approach that planarizes each quad face independently is given in figure 9.

Table 1: Optimization tradeoffs

Optimization	A	B	C	D	E
Average kappa angle	2.05°	1.9°	1.7°	1.3°	1.03°
Maximal kappa angle	6.93°	5.5°	5.1°	4.4°	3.72°
Average alpha angle	121.4°	118.7°	116.9°	112.4°	110.6°
Minimal alpha angle	106.5°	105.4°	102.1°	100.1°	100.3°
Average surface deviation	13.5mm	30.9mm	38.6mm	42.3mm	46.2mm

Below we give a summary of the different constraints we use in our optimization. These constraints are equipped with weights that allow balancing the trade-offs inherent in our over-constrained optimization. Please refer to [Deuss et al. 2015] for a derivation of the constraints and a more detailed description of their implementation. An open-source implementation of the solver can be found at <http://shapeop.org/>.

To optimize our plate assembly we use the following constraints:

- *Planarity* of the four vertices of each quadrilateral ensures fabricability. We use a high weight to respect the very high stiffness of the LVL plates.
- *Closeness* links the quads to the target surface. We set high weights for vertices on the boundary to match the site requirements. For interior vertices we use lower weights so that elements can adapt in size and shape, if necessary to satisfy fabrication and assembly objectives.
- *Angle* bounds the angles of each quad face to preserve the initial rhomboid shape and avoid rectangular faces.
- *Parallelogram* is used with a low weight for aesthetic reasons on the non-boundary elements.
- *Divergence* is a new constraint that we introduce specifically to handle our disconnected plate arrangement. This constraint couples adjacent plates by minimizing the distance between neighboring vertices. The projection operator for this constraint is simply given as the mean position of two vertices, applied on each pair of adjacent vertices as defined by the topology of the grid layout.

The global optimization in figure 10 and table 1 reduces the average kappa angles κ_{mean} by up to 50%, compared to the local optimization. This is possible through a trade-off between multiple parameters. We allow for a controlled deviation from the base surface and for the alpha angles. Option C shows a balanced compromise, where κ_{mean} is reduced by 17%. At the same time α_{mean} is well preserved with a loss of only 2.2% compared to the local optimization (Option A), avoiding any negative effects on the mechanical strength of the joints.

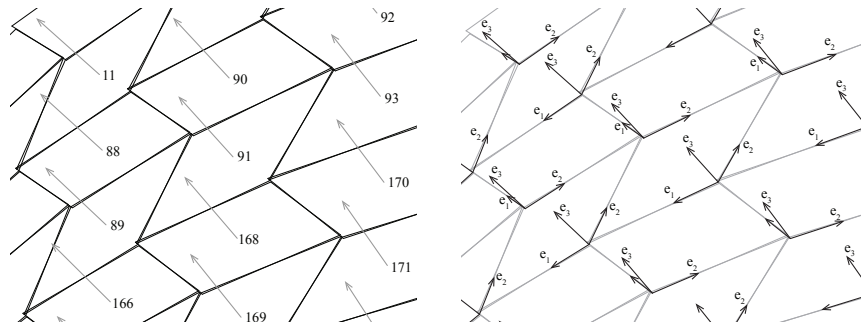


Figure 11: left: disconnected planar faces, right: frames for plate generation

We run the local-global solver that iterates between constraint projection and global linear solver for 50-200 iterations. The output of the solver is then feed into a second algorithm that creates the two layer shell structure. We generate the four plates per face, based on local frames that we obtain from the disconnected quadrilaterals (Figure 11). The frames show the mid-layer planes of the shear block plates W0: e_1, e_3 and W1: e_2, e_3 and the insertion direction $\vec{v} = (e_1 + e_2)/2$. For the shell plate quads, one corner lies along e_3 , while the other corners are found through an intersection with the shear block planes of the neighboring segments. The final result is shown in Figure 12.

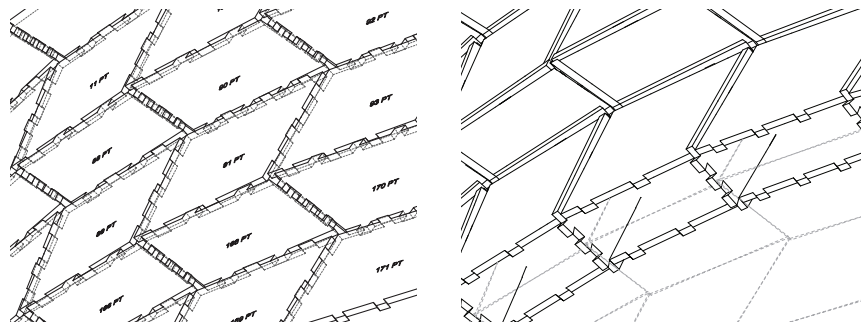


Figure 12: left: upper shell plates, right: cross-section view

4 Fabrication

In order to test the fabrication and assembly, a prototype of the structure was built using 15mm birch plywood panels (scale 1:2.66). Figure 13 shows the location of the prototype within the first double-curved shell of our project. It shows the assembly of 4x7 hexahedron-shaped segments, consisting of 112 interlocking plates connected entirely with through-tenon and dovetail joints.

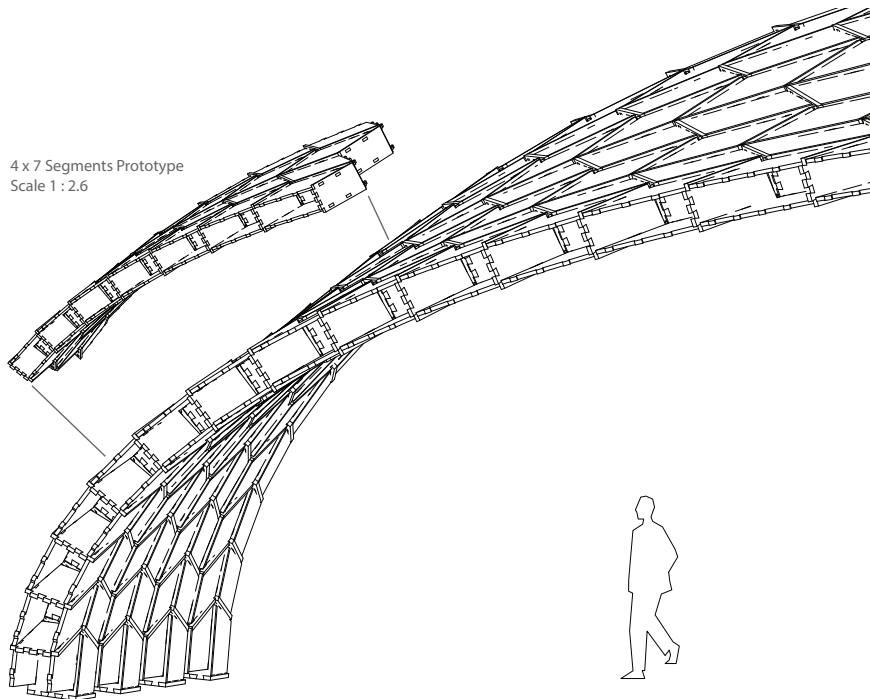


Figure 13: Isometry of arch 1 with location of Prototype A (scale 1 : 2.66)

The main algorithm generates the geometry of each plate through an upper and lower polygon contour. On the shear plates, there are additional polygon contours for the joint slots. For the fabrication of the parts, the polygon contours for each plate are laid out on the World XY plane.

A second algorithm was used for the cutting of the parts with a 5-axis milling machine. It generates the G-Code through a loft-like 3D offset of the plate contour polygons. On concave corners, notches are added automatically. [Robeller and Weinand 2016a]

The total contour or cutting path length of the prototype (28 segments, 112 plates) is 217 meters. Parts were cut with 4 infeeds at 5m/min (2x roughing without notches, 2x final cut with notches). Compared to a plate contour without integral joints, the contour length with the joints increases by 20% for the shell plates and 100% for the shear plates, which contain all of the slots.

On the full-scale structure, built from LVL plates with a thickness of 40mm, the 1,248 plates of the first and largest arch add up to a total area of $1,063m^2$ (without off-cuts), a volume of $43m^3$ and a self-weight of 32 tons.

The prototype was assembled lying on its side, inserting the tight fitting pieces with a small mallet as shown in Figure 14. A similar prefabrication strategy is planned for the full-scale structure, dividing the 23 shells into an average of 6 pre-

fabricated modules per arch, with a maximum transportation size of 20x2 meters. In between these large modules, through-tenon joints cannot be used for the assembly, because no common assembly direction can be found. Instead, additional shear plates can be added and connected with metal fasteners on site. This strategy would require regular metal fastener joints on 17% of the edge-to-edge connections on the first arch.



Figure 14: 4x7 segment prototype at scale 1:2.6

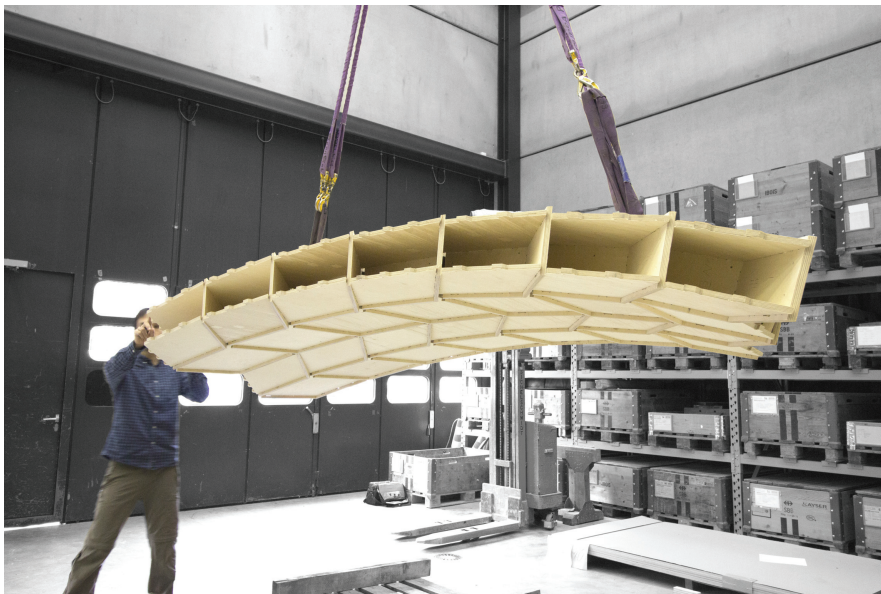


Figure 15: 4x7 segment prototype, fabricated from 15mm birch veneer panels (scale 1:2.6)

5 Conclusion

With his Gaussian vault structures, Eladio Dieste developed a highly elegant and efficient structural system, taking advantage of local resources and technology at his time. In the same spirit, the new construction system in this paper presents a contemporary re-interpretation of a double-curved shell structure using timber, a locally sourced material which addresses the contemporary shell for sustainable building structures.

Dieste's masonry shells were based on the material and its connections, which could not resist bending forces. This was addressed through the form of the shells, but it also put a great outward thrust on the supports, requiring substantial reinforcements. Our new construction system uses integrally attached timber plates, with different material and joint properties. Our joints can resist bending forces, this reflects in the different form of our shells, which reduces horizontal forces on the supports.

While previous projects introduced dovetail joints for the connection of timber plates, the through-tenon joints provide a high resistance to bending forces. Like the dovetail joints, the through-tenons are also prismatic joints and reduce the mobility of parts to a single motion path.

The use of prismatic joints, fabricated with a 5-axis CNC enabled cutting method, allows us to integrate the assembly instructions into the shape of the plates. Therefore, our construction system does not require a mould, which is crucial for the case study project with its 23 individually shaped shells.

The tiling with trapezoidal shaped hexahedron segments was chosen to optimize the assembly of the structure, the mechanical strength of the joints and the transfer of forces within the structure.

A rotation of the tabs allows for the piece-by-piece assembly of small plates, connecting multiple edges simultaneously. We have analyzed the influence of this rotation on the shear strength of the joints and optimized the shape of our plates based on the results.

The alternation of the joint rotation in every second row avoids long range escape paths, supporting our strategy of blocking parts with one another, using their form to reduce or replace the need for additional fasteners.

At the same time, the alternating trapezoidal shape of the segments results in an alternating rotation of all edges across the direction of span on all shells. The length of these edges is increased and continuous bending axes are avoided.

The research underlines the need for close interdisciplinary collaboration of architects, computer scientists, and engineers in the development of new types of sustainable lightweight structures, which are equally optimized for fast and precise assembly and for structural efficiency.

Acknowledgments

This research was supported by the NCCR Digital Fabrication, funded by the Swiss National Science Foundation. (NCCR Digital Fabrication Agreement #51NF40-141853))

References

- ANDERSON, S. 2004. *Eladio Dieste: Innovation in Structural Art*. Princeton Architectural Press.
- BOUAZIZ, S., DEUSS, M., SCHWARTZBURG, Y., WEISE, T., AND PAULY, M. 2012. Shape-up: Shaping discrete geometry with projections. *Comput. Graph. Forum* 31, 5 (Aug.).
- DEUSS, M., DELEURAN, A. H., BOUAZIZ, S., DENG, B., PIKER, D., AND PAULY, M. 2015. *Modelling Behaviour: Design Modelling Symposium 2015*. Springer International Publishing, Cham, ch. ShapeOp—A Robust and Extensible Geometric Modelling Paradigm, 505–515.
- KRIEG, O. D., SCHWINN, T., MENGES, A., LI, J.-M., KNIPPERS, J., SCHMITT, A., AND SCHWIEGER, V. 2015. *Advances in Architectural Geometry 2014*. Springer International Publishing, Cham, ch. Biomimetic Lightweight Timber Plate Shells: Computational Integration of Robotic Fabrication, Architectural Geometry and Structural Design, 109–125.
- LA MAGNA ET AL., R. 2013. From nature to fabrication: Biomimetic design principles for the production of complex spatial structures. *International Journal of Spatial Structures* 28, 01, 27–40. Doi: 10.1260/0266-3511.28.1.27 (ISSN 0266-3511).
- LI, J.-M., AND KNIPPERS, J. 2015. Segmental timber plate shell for the landesgartenschau exhibition hall in schwäbisch gmünd—the application of finger joints in plate structures. *International Journal of Space Structures* 30, 2, 123–140.
- LIU, Y., POTTMANN, H., WALLNER, J., YANG, Y.-L., AND WANG, W. 2006. Geometric modeling with conical meshes and developable surfaces. *ACM Trans. Graph.* 25, 3 (July), 681–689.
- PEDRESCHI, R., AND THEODOSSOPOULOS, D. 2007. The double-curvature masonry vaults of eladio dieste. *Proceedings of the ICE - Structures and Buildings* 160, 1 (2), 3–11.
- POTTMANN, H., EIGENSATZ, M., VAXMAN, A., AND WALLNER, J. 2015. Architectural geometry. *Computers and Graphics* 47, 145–164.
- ROBELLER, C., AND WEINAND, Y. 2015. Interlocking folded plate – integral mechanical attachment for structural wood panels. *International Journal of Space Structures* 30, 2, 111–122.

- ROBELLER, C., AND WEINAND, Y. 2016. A 3d cutting method for integral 1dof multiple-tab-and-slot joints for timber plates, using 5-axis cnc cutting technology. In *Proceedings of the World Conference on Timber Engineering WCTE 2016*.
- ROBELLER, C., AND WEINAND, Y. 2016. *Robotic Fabrication in Architecture, Art and Design 2016*. Springer International Publishing, Cham, ch. Fabrication-Aware Design of Timber Folded Plate Shells with Double Through Tenon Joints, 166–177.
- ROCHE, S., MATTONI, G., AND WEINAND, Y. 2015. Rotational stiffness at ridges of timber folded-plate structures. *International Journal of Space Structures* 30, 2, 153–168.
- ROCHE, S., ROBELLER, C., HUMBERT, L., AND WEINAND, Y. 2015. On the semi-rigidity of dovetail joint for the joinery of lvl panels. *European Journal of Wood and Wood Products* 73, 5, 667–675.
- WHITNEY, D. 2004. *Mechanical Assemblies: Their Design, Manufacture, and Role in Product Development*. No. Bd. 1 in *Mechanical Assemblies: Their Design, Manufacture, and Role in Product Development*. Oxford University Press.

Authors' address:

Christopher Robeller (christopher.robeller@epfl.ch): EPFL Laboratory for Timber Construction IBOIS / Station 18 — CH 1015 Lausanne.

Mina Konakovic (mina.konakovic@epfl.ch): EPFL Computer Graphics Laboratory LGG / Station 14 — CH 1015 Lausanne.

Mira Dedijer (mira.dedijer@epfl.ch): EPFL Laboratory for Timber Construction IBOIS / Station 18 — CH 1015 Lausanne.

Yves Weinand (yves.weinand@epfl.ch): EPFL Laboratory for Timber Construction IBOIS / Station 18 — CH 1015 Lausanne.

Mark Pauly (mark.pauly@epfl.ch): EPFL Computer Graphics Laboratory LGG / Station 14 — CH 1015 Lausanne.